ELSEVIER

Composites: Part B 33 (2002) 567–578

composites
Part B: engineering

www.elsevier.com/locate/compositesb

The effects of geometric parameters on the failure strength for pin-loaded multi-directional fiber-glass reinforced epoxy laminate

Buket Okutan*

Department of Mechanical Engineering, Dokuz Eylül University, 35100 Bornova, Izmir, Turkey

Received 17 January 2002; revised 26 July 2002; accepted 28 July 2002

Abstract

A numerical and experimental study was carried out to determine the failure of mechanically fastened fiber-reinforced laminated composite joints. E/glass–epoxy composites were manufactured to fabricate the specimens. Mechanical properties and strengths of the composite were obtained experimentally. Tests have been carried out on single pinned joints in $[0/90/0]_s$ and $[90/0/90]_s$ laminated composites. A parametric study considering geometries was performed to identify the failure characteristics of the pin-loaded laminated composite. Data obtained from pin-loaded laminate tests were compared with the ones calculated from a finite element model (PDNLPIN computer code). Damage accumulations in the laminates were evaluated by using Hashin's failure criteria combined with the proposed property degradation model. Based on the results, ply orientation and geometries of composites could be crucial for pinned laminated composite joints.

Keywords: A. Glass fibers; Non-linear behavior; Pin; Stress/strain curves; Strength

1. Introduction

A structural joint represents a critical element in the step of design. In all cases a significant weight penalty is incurred by the presence of joints in composite structures; furthermore, premature failures have been experienced too frequently. Consequently, the design of efficient structural attachments represents one of the major challenges in the development of composite structures. Because of its generic nature, the design is deserving of separate treatment as a case study.

The design and testing of joint components, together with some theoretical and experimental work, are important because the ability of joint elements is central to a full exploitation of high performance of fiber-reinforced composites. Due to the significance of the problem, pin-loaded laminated composite plates have been studied by using analytical [1–3], numerical [4–13] and experimental [14–20] methods in the literature. Several approaches have been used to predict the stresses, failure strengths and failure modes of composite laminates containing pin-loaded hole.

It is very important to fundamentally characterize the damage mechanisms of pinned composite joints as a function of geometry and ply orientation. An optimal design in composite structures can only be achieved by thorough understanding of the failure mechanisms in laminated composites. Therefore, the objective of this study is to assess, both numerically and experimentally, the effects of joint geometry and ply orientation on the failure strength and on failure mode. The knowledge of the failure strength would help in selecting the appropriate joint size in a given application. $[0/90/0]_s$ and $[90/0/90]_s$ stacking sequences were selected for such an analysis because it is desired to see the effects of relative proportions of the 0 and 90° layers on the joint strength.

2. Statement of the problem

Consider a rectangular composite plate of length L, thickness t and width W with a hole of diameter D. The hole is at a distance E from the free edge of the plate. The configuration of composite plate is shown in Fig. 1. A tensile load is applied at the hole free edge of the plate resisted by the pin.

Load is applied gradually. During loading, the plate is

* Tel.: +90-3884000/2255.
E-mail address: buket@deu.edu.tr (B. Okutan).

1359-8368/02/$ - see front matter © 2002 Published by Elsevier Science Ltd.
PII: S1359-8368(02)00054-9

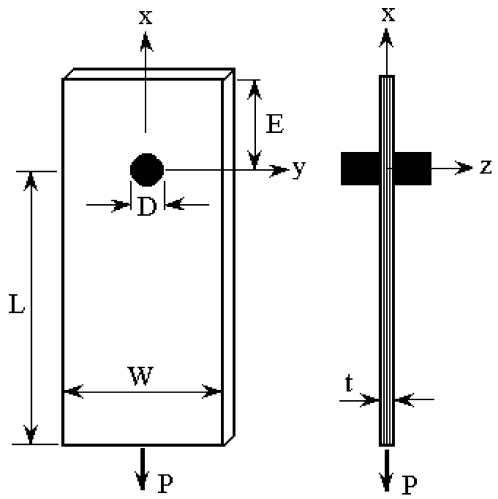

Fig. 1. Geometry of specimen with pin-loaded hole.

allowed to deform until it collapses, at which point the plate cannot sustain any additional load. It is desired to find;

- The load–displacement tensile response for each specimen
- The damage progression before final failure
- The ultimate failure load
- The corresponding modes of failure.

3. Testing

3.1. Manufacturing of composite laminates

The laminates manufactured for the tests were made from E glass-fiber and epoxy resin CY225 mixed hardener HY225 in the mass ratio of 100:80. Subsequent plies were placed one upon another to obtain required stacking sequences ($[0/90/0]_s$ and $[90/0/90]_s$). A hand roller was used to distribute resin, compact plies and remove entrapped air. The mold and lay-up were covered with a release film to prevent the lay-up from bonding to the mold surface. Then resin-impregnated fibers were placed in the mold for curing. The glass fiber and epoxy were cured at 120 °C under a pressure of 0.2 MPa. This temperature was held constant for 4 h for the first period. Afterwards, the temperature was decreased to 100 °C and held constant for 2 h for the second period. After the second period, the laminates were cooled to room temperature. The finished specimens had an average thickness of 3.3 mm and length 50 mm with a fiber volume fraction of 57%.

3.2. Material characterization

Tensile tests have been performed on longitudinal $[0°]_6$ and transverse $[90°]_6$ rectangular specimens to determine Young's moduli (E_1), (E_2); Poisson's ratio (ν_{12}); longitudinal tensile strength (X_t) and transverse tensile strength (Y_t), according to the ASTM D3039-76 [21] standard test method as reported in Table 1.

The in-plane shear strength of the material has been measured using Iosipescu shear test [22,23]. The shear stress–strain data can be generated and the corresponding modulus and strength can be found from resulting stress–strain curve. A typical shear response was represented in Fig. 2. It can be seen that the response is highly non-linear. The constant (α), which is necessary to observe non-linear elastic material behavior, is calculated by non-linear shear–strain relation [24]. This relation is written as

$$\gamma_{12} = \tau_{12}/G_{12} + \alpha\tau_{12}^3 \tag{1}$$

As another test, following the ASTM 3518 standard [25], the 45° off-axis tensile test [26] was used to measure the in-plane shear response of the composite. The shear modulus G_{12} obtained by this method and Iosipescu test were nearly the same and were given separately in Table 1.

An additional test to find shear strength S was performed using 'T shape' specimen. The specimen dimensions and geometry were shown in Fig. 3. This method was used to verify shear strength of the unidirectional lamina obtained by Iosipescu test method. No special fixture was needed and manufacturing of the specimen was simple [27–29]. Minimum clearance was left to prevent bending and to provide contact between specimen and support. The load at rupture (P_{ult}) was taken and shear strength was calculated by the following equation.

$$S = \frac{P_{ult}}{2ht} \tag{2}$$

In this equation, $h = 5$ mm, $L_T = 80$ mm, $a = 10$ mm and $b = 40$ mm were taken. The values of shear strengths

Table 1
Properties of glass-fiber/epoxy composite

	Symbol (units)	Unidirectional
Moduli parameters		
Density	ρ (g/cm^3)	1.506
Longitudinal modulus	E_1 (MPa)	44,000 ($\pm$560)
Transverse modulus	E_2 (MPa)	10,500 ($\pm$420)
Shear modulus	G_{12} (MPa)	$3740^{\text{Iosipescu}}$ ($\pm$335) $3880^{45\ \text{off-axis}}$ ($\pm$360)
Poisson's ratio	ν_{12} (–)	0.36
Material non-linearity parameter	α (MPa)$^{-3}$	7.17×10^{-8} Iosipescu ($\pm 1.03 \times 10^{-9}$)
Strength parameters		
Longitudinal tension	X_t (MPa)	800 ($\pm$59)
Longitudinal compression	X_c (MPa)	350 ($\pm$42)
Transverse tension	Y_t (MPa)	50 ($\pm$4.35)
Transverse compression	Y_c (MPa)	125 ($\pm$9.34)
Shear strength	S (MPa)	$120^{\text{Iosipescu}}$ ($\pm$15.28) $115^{\text{T specimen}}$ ($\pm$18.35)

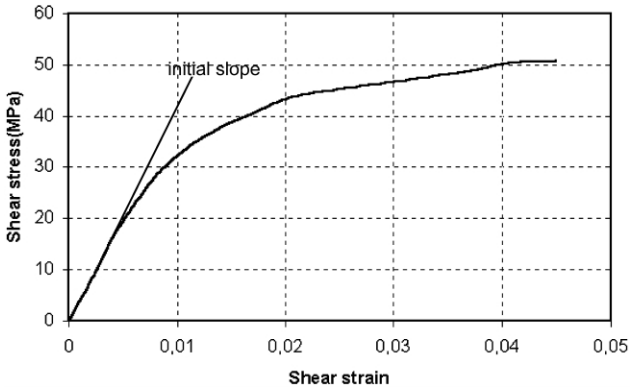

Fig. 2. Typical stress–strain curve of glass/epoxy laminate.

obtained by T-shear test set-up and Iosipescu shear test method agreed well as can be seen in Table 1. In the numerical calculations the values of shear modulus and shear strength obtained from Iosipescu shear test were used.

In this study, the specimen with a very short but unsupported gage-length was used. Compression tests have been performed using $[0°]_6$ and $[90°]_6$ specimens with 6.4 mm width and 12.7 mm gage length. Compressive load was applied to the specimen and maximum failure load was recorded to find longitudinal and transverse compression strengths X_c and Y_c, respectively.

3.3. Joint testing configuration

In the tensile test, different width/diameter (W/D) and edge distance/diameter (E/D) ratios were considered. Each plate was cut and prepared with a single circular hole, centrally placed with respect to the width and at a predetermined distance from the end. The specimens were 5 mm drilled to give 20 specimens with E/D = 1 to 5 and W/D = 2 to 5. The specimens were tested in Mitutoya testing machine of 50 kN load capacity, the 0° layer being aligned with the load.

A double-lap fixture shown in Fig. 4 was used to perform the tests. All specimens were mounted in the testing machine using a set of test fixtures specially designed for this experiment and loaded at a constant crosshead rate (0.5 mm/min) to minimize any catastrophic failure and to

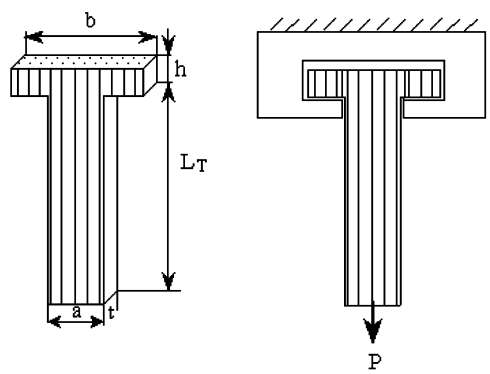

Fig. 3. Shear test setup.

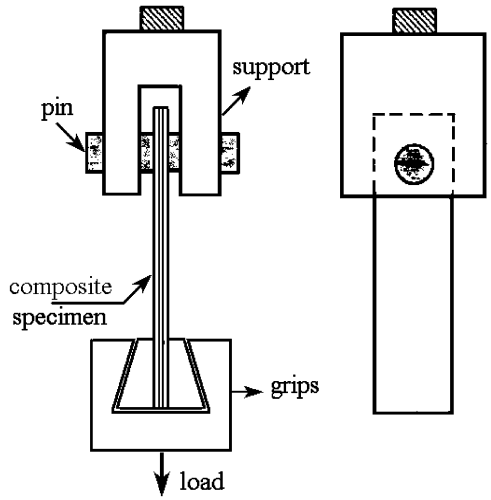

Fig. 4. Schematic diagram for double-lap, single pin joint.

allow the time possible for observation of damage and its progression. For each test, applied load and pin displacement were continuously recorded from the chart recorder attached to the testing machine. The magnitude of the applied load was measured by using a load cell mounted on the testing machine. The displacement of bottom grip was also recorded during the tests. Specimens were tested to final failure. It was observed how failure is affected by geometry, specially the variation of plate width and end distance.

4. Finite element modeling

The behavior of the pin-loaded joint was predicted using a progressive two-dimensional finite element model developed by Larry Lessard [8]. In the finite element model, only half of the plate was modeled, since the geometry and loading conditions of the cross-ply laminates were symmetric with respect to the y–z plane.

It was assumed that,

(1) The laminate is symmetric with respect to its mid-plane and applied load is in-plane.
(2) The pin is considered to be perfectly rigid with zero clearance.
(3) The pin-composite interaction is assumed to be frictionless.

Meshing and boundary conditions for the model can be seen in Fig. 5. As can be seen from this figure, a large number of elements were used at the edge of the hole to obtain a better accuracy of the stresses. Nodes on the vertical centerline were restrained to move only along the vertical y-direction ($u_x = 0$). To simulate the pin, radial boundary conditions were used on the topside of the hole.

The model of the joint problem is an integration of three major components: stress analysis, failure criteria

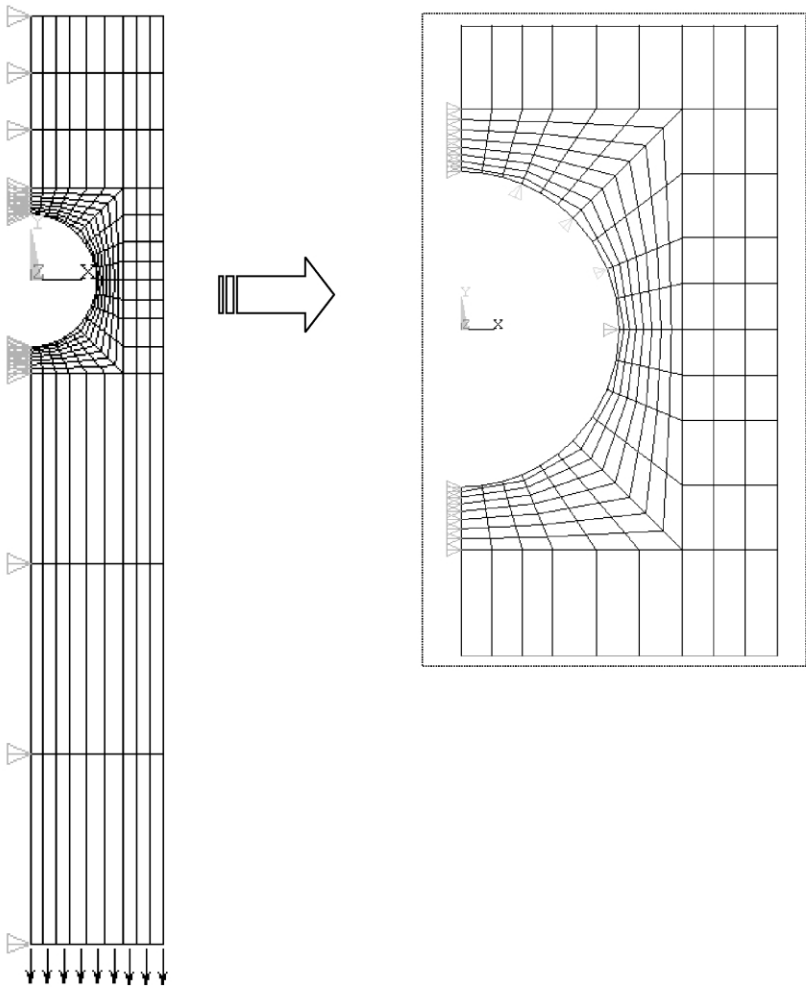

Fig. 5. Mesh representing and boundary conditions.

and property degradation rules. In the first step, the material properties, physical properties and appropriate boundary conditions of the problem are provided and load increment is selected. At each load step, non-linear finite element analysis is performed until a converged solution is obtained. The stress analysis uses standard laminated composites plate theory to describe the stress–strain behavior of the composite material. The stresses at each material integration point are utilized for failure analysis. Failure criteria are tested at each load step. The effect of material non-linearity on the mathematical forms of failure criteria is taken into account. In the case of failure, material properties of failed plies are reduced according to the mode failure and the appropriate property degradation rule. Stresses are then redistributed and re-examined for any additional failures under the same load. Convergence at a load step without additional failure allows the next load step to be pursued and the procedure continues until a point where excessive damage is reached. Usually this means failure has propagated to a specimen edge and applied load cannot redistribute itself around damaged areas.

4.1. Failure criteria

In this investigation, Hashin failure criteria [30] were used. In the following, for five different failure modes (matrix tensile and compression, fiber-matrix shearing, fiber tensile and compression failure), five failure criteria were explained. A complete set of material degradation rules was explained for each mode of failure [8].

4.2. Matrix tensile failure

For predicting matrix tensile failure of a unidirectional ply under static stress, the criterion can be expressed

$$\left(\frac{\sigma_2}{Y_t}\right)^2 + \frac{\int_0^{\gamma_{12}} \tau_{12}\, d\gamma_{12}}{\int_0^{\gamma_{12}^u} \tau_{12}\, d\gamma_{12}} > 1 \qquad \text{and} \qquad \sigma_2 > 0 \tag{3}$$

where σ_2 and τ_{12} are the transverse tensile stress and shear stress in each layer, respectively. Y_t is the transverse tensile strength and γ_{12} is the ply shear strain. By considering

the non-linear shear stress–strain behavior of the unidirectional ply in x–y plane, the second term of Eq. (3) appear in integral form. In the denominator of second term, the upper limit of integration is the ply ultimate shear strain. By introducing the ply shear stress–shear strain relationship of Eq. (1), it can be obtain

$$\left(\frac{\sigma_2}{Y_t}\right)^2+\frac{\dfrac{\tau_{12}^2}{2G_{12}}+\dfrac{3}{4}\alpha\tau_{12}^4}{\dfrac{S^2}{2G_{12}}+\dfrac{3}{4}\alpha S^4}>1 \qquad \text{and} \qquad \sigma_2>0 \tag{4}$$

where G_{12} is the initial shear modulus, and α is the shear non-linearity parameter (found experimentally) and S is the ply shear strength.

If non-linearity is weak, $\alpha\to 0$, then it is easy to show that Eq. (4) will reduce to the linear failure form of Eq. (5) as proposed by Hashin [30]. Noting that the material non-linearity affects only the shear stress–strain relationship.

$$\left(\frac{\sigma_2}{Y_t}\right)^2+\left(\frac{\tau_{12}}{S}\right)^2>1 \qquad \sigma_2>0 \tag{5}$$

Similar to matrix tensile failure, the other failure criteria may be converted from linear to non-linear form.

When matrix tensile failure occurs in a ply, then the material properties in that ply are degraded. Both before and after the application of the degradation rule, the plane stiffness matrix is

$$\begin{bmatrix} \dfrac{E_1}{1-\upsilon_{12}\upsilon_{21}} & \dfrac{E_1\upsilon_{21}}{1-\upsilon_{12}\upsilon_{21}} & 0 \\ \dfrac{E_2\upsilon_{12}}{1-\upsilon_{12}\upsilon_{21}} & \dfrac{E_2}{1-\upsilon_{12}\upsilon_{21}} & 0 \\ 0 & 0 & G_{12} \end{bmatrix} \to \begin{bmatrix} E_1 & 0 & 0 \\ 0 & 0 & 0 \\ 0 & 0 & G_{12} \end{bmatrix} \tag{6}$$

4.3. Matrix compression failure

Matrix static failure in compression has the following form

$$\left(\frac{\sigma_2}{Y_c}\right)^2+\frac{\displaystyle\int_0^{\gamma_{12}}\tau_{12}\,\mathrm{d}\gamma_{12}}{\displaystyle\int_0^{\gamma_{12}'}\tau_{12}\,\mathrm{d}\gamma_{12}}>1 \qquad \text{and} \qquad \sigma_2<0 \tag{7}$$

where Y_c is the transverse compressive strength. Again by considering the ply shear stress–strain relationship of Eq. (1) we obtain:

$$\left(\frac{\sigma_2}{Y_c}\right)^2+\frac{\dfrac{\tau_{12}^2}{2G_{12}}+\dfrac{3}{4}\alpha\tau_{12}^4}{\dfrac{S^2}{2G_{12}}+\dfrac{3}{4}\alpha S^4}>1 \qquad \text{and} \qquad \sigma_2<0 \tag{8}$$

If non-linearity is weak, $\alpha\to 0$, then Eq. (8) will reduce to the linear failure form as follow

$$\left(\frac{\sigma_2}{Y_c}\right)^2+\left(\frac{\tau_{12}}{S}\right)^2>1 \text{ and} \qquad \sigma_2<0 \tag{9}$$

When the matrix compression failure occurs in a ply, then the material properties in that ply are degraded as follows:

$$\begin{bmatrix} \dfrac{E_1}{1-\upsilon_{12}\upsilon_{21}} & \dfrac{E_1\upsilon_{21}}{1-\upsilon_{12}\upsilon_{21}} & 0 \\ \dfrac{E_2\upsilon_{12}}{1-\upsilon_{12}\upsilon_{21}} & \dfrac{E_2}{1-\upsilon_{12}\upsilon_{21}} & 0 \\ 0 & 0 & G_{12} \end{bmatrix} \to \begin{bmatrix} E_1 & 0 & 0 \\ 0 & 0 & 0 \\ 0 & 0 & G_{12} \end{bmatrix} \tag{10}$$

4.4. Fibers/matrix shearing failure

This mode of failure is important for compression failure dominated by shear stresses, and has the following form:

$$\left(\frac{\sigma_1}{X_c}\right)^2+\frac{\dfrac{\tau_{12}^2}{2G_{12}}+\dfrac{3}{4}\alpha\tau_{12}^4}{\dfrac{S^2}{2G_{12}}+\dfrac{3}{4}\alpha S^4}>1 \qquad \text{and} \qquad \sigma_1<0 \tag{11}$$

Linear form of Eq. (11)

$$\left(\frac{\sigma_1}{X_c}\right)^2+\left(\frac{\tau_{12}}{S}\right)^2>1 \qquad \text{and} \qquad \sigma_1<0 \tag{12}$$

where σ_1 is the longitudinal stress, X_c is the longitudinal compressive strength of a unidirectional ply under static stresses, and τ_{12} is shear stress and S shear strength.

In fiber/matrix shearing failure mode, while the material can still carry load in the fiber and matrix directions, in-plane shear stress can no longer be carried.

$$\begin{bmatrix} \dfrac{E_1}{1-\upsilon_{12}\upsilon_{21}} & \dfrac{E_1\upsilon_{21}}{1-\upsilon_{12}\upsilon_{21}} & 0 \\ \dfrac{E_2\upsilon_{12}}{1-\upsilon_{12}\upsilon_{21}} & \dfrac{E_2}{1-\upsilon_{12}\upsilon_{21}} & 0 \\ 0 & 0 & G_{12} \end{bmatrix} \to \begin{bmatrix} E_1 & 0 & 0 \\ 0 & E_2 & 0 \\ 0 & 0 & 0 \end{bmatrix} \tag{13}$$

4.5. Fiber tensile failure

For fiber tensile failure of a unidirectional ply, the following criterion is used:

$$\left(\frac{\sigma_1}{X_t}\right)^2+\frac{\dfrac{\tau_{12}^2}{2G_{12}}+\dfrac{3}{4}\alpha\tau_{12}^4}{\dfrac{S^2}{2G_{12}}+\dfrac{3}{4}\alpha S^4}>1 \qquad \text{and} \qquad \sigma_1>0 \tag{14}$$

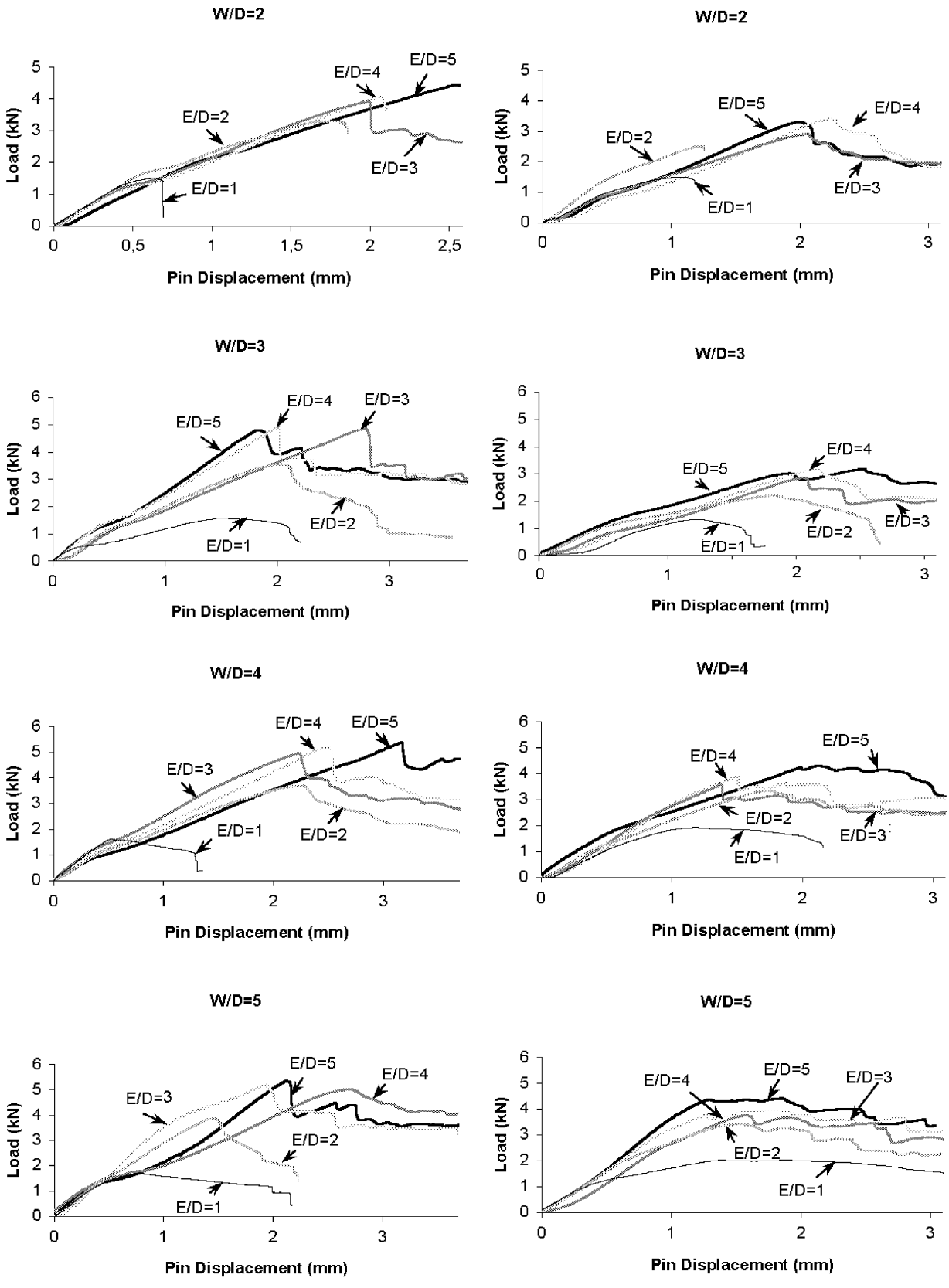

Fig. 6. Load/displacement curves for $[0/90/0]_s$ and $[90/0/90]_s$ laminates.

Linear form of Eq. (14)

$$\left(\frac{\sigma_1}{X_t}\right)^2+\left(\frac{\tau_{12}}{S}\right)^2>1 \qquad \text{and} \qquad \sigma_1>0 \tag{15}$$

where X_t is the longitudinal fiber tensile strength of a unidirectional ply under static stresses in fiber direction.

Since fibers are the primary load carrying elements of fiber-reinforced composites, failure of fibers is linked directly to the final failure of composites. Therefore, when fiber failure mode occurs in a ply, the material losses all of its properties as follow

$$\begin{bmatrix} \frac{E_1}{1-\upsilon_{12}\upsilon_{21}} & \frac{E_1\upsilon_{21}}{1-\upsilon_{12}\upsilon_{21}} & 0 \\ \frac{E_2\upsilon_{12}}{1-\upsilon_{12}\upsilon_{21}} & \frac{E_2}{1-\upsilon_{12}\upsilon_{21}} & 0 \\ 0 & 0 & G_{12} \end{bmatrix} \rightarrow \begin{bmatrix} 0 & 0 & 0 \\ 0 & 0 & 0 \\ 0 & 0 & 0 \end{bmatrix} \tag{16}$$

4.6. Fiber compression or bearing failure

Fiber compression failure is independent of shear stresses. This mode of failure deals with failure of fibers in compression. For the pinned-joint problem, this mode of failure may occur just ahead of the pin and the joint may still be able to carry load. The damaged zone of the pin may still transfer load-allowing failure to propagate further ahead of the pin. For predicting fiber compression failure the criterion can be expressed as

$$\left(\frac{\sigma_1}{X_c}\right)^2>1 \qquad \sigma_1<0 \tag{17}$$

As shown in Eq. (17), for this mode of failure, the interaction terms from shear stresses are not considered. When the fiber compression failure occurs in a ply, then the all-material properties in that ply are reduced to zero as shown in Eq. (16).

5. Results and discussion

5.1. Experimental results

The general behavior of the composites was obtained from the load/displacement chart from the testing machine. The load/displacement curves for $[0/90/0]_s$ and $[90/0/90]_s$ laminates were shown in Fig. 6. From this figure, it can be said that the specimens of $[0/90/0]_s$ laminate were able to support between 400 and 4300 N after first failure occurred. The displacement at which the last failure occurred could be seen to vary from 0.6 mm for narrow specimens with short end distances to 3.1 mm for wide specimens with long end distances. In a similar way, the $[90/0/90]_s$ laminate specimens were able to withstand between 800 and 2500 N after first failure occurred. The displacement at which last failure occurred can be seen to vary from 1.1 mm for narrow specimens with short end distances to 2.7 mm for wide specimens with long end distances. Maximum load sustained by the specimen was used as a measure joint strength.

As the pin displacement increased, the load increased in an almost linear manner. Then, failure started at different loads for different geometries and ply orientations and the load reached a peak (first peak). After the first peak, the load displacement curves showed valleys, peaks and plateaus depending on types of ply orientations and geometry. The pin hole was found to suffer permanent deformation increased progressively with load.

In this investigation, while laminated composite plates were loaded to final failure, ultimate failure was either net-tension or shear-out, there was always evidence of bearing failure for the different geometric dimensions and lay-ups. For the $[0/90/0]_s$ laminate, failure modes were found as bearing mode when the E/D ratio is greater than 3. For the small value of 3, the mode is found as shear-out that is a weak type of failure. Similar result was obtained for the critical W/D ratio. For the $[90/0/90]_s$ laminate, it was found that the critical E/D ratio was 4 for $W/D = 2$ and 3 and the critical E/D ratio was about 2 for $W/D = 3$ and 4. Prior to reaching the critical E/D values, net-tension failure was observed in all specimens except for the ones with $E/D = 1$, which displayed a shear-out failure mode. Photographs of typical failures in $[0/90/0]_s$ and $[90/0/90]_s$ laminates were shown in Fig. 7.

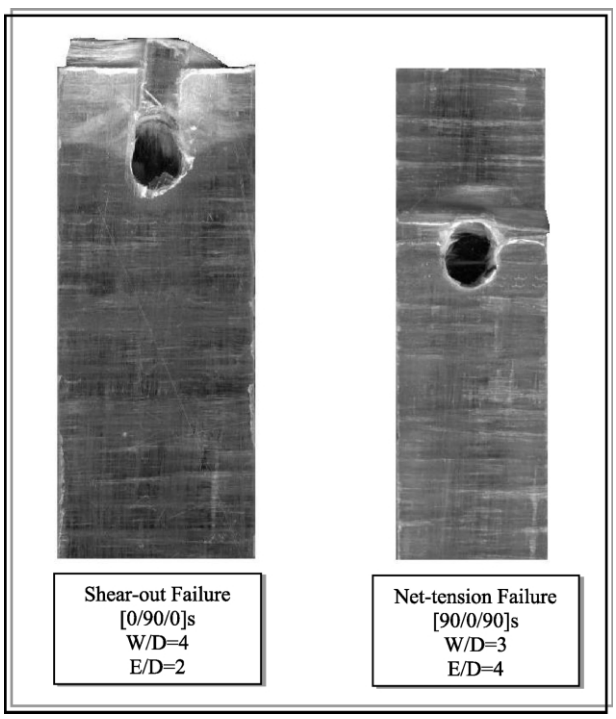

Fig. 7. Typical failures in $[0/90/0]_s$ and $[90/0/90]_s$ laminates.

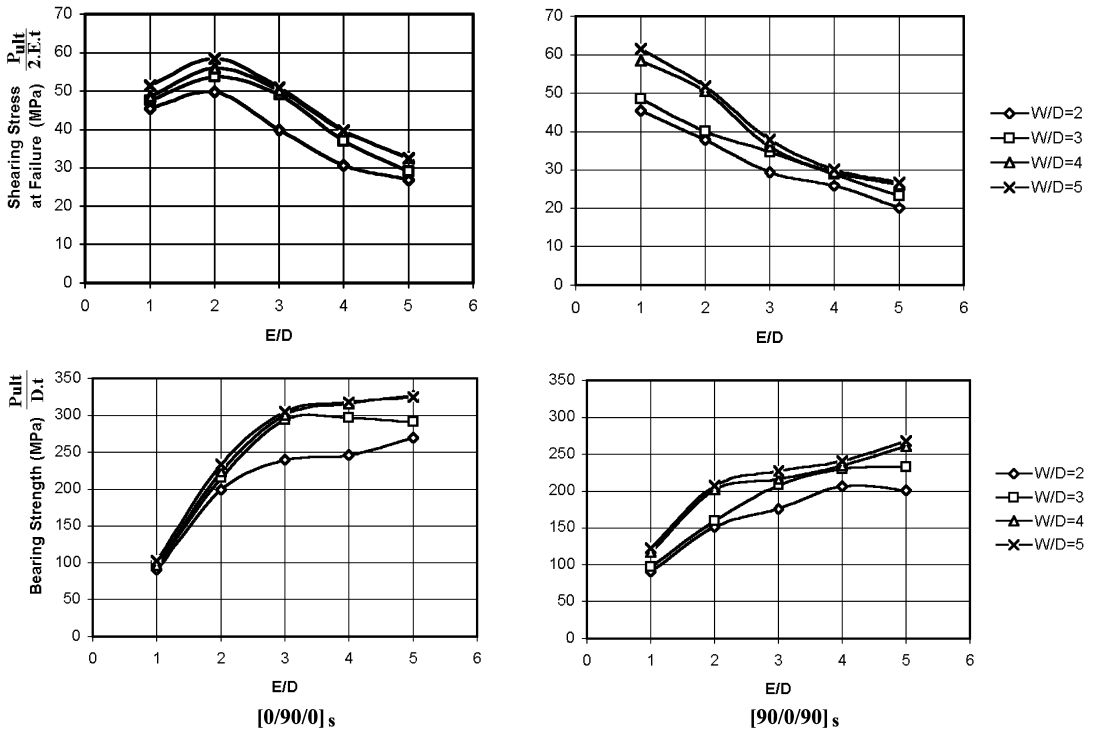

Fig. 8. The effect of edge distance to diameter ratio on the shearing and bearing strength for $[0/90/0]_s$ and $[90/0/90]_s$ laminates.

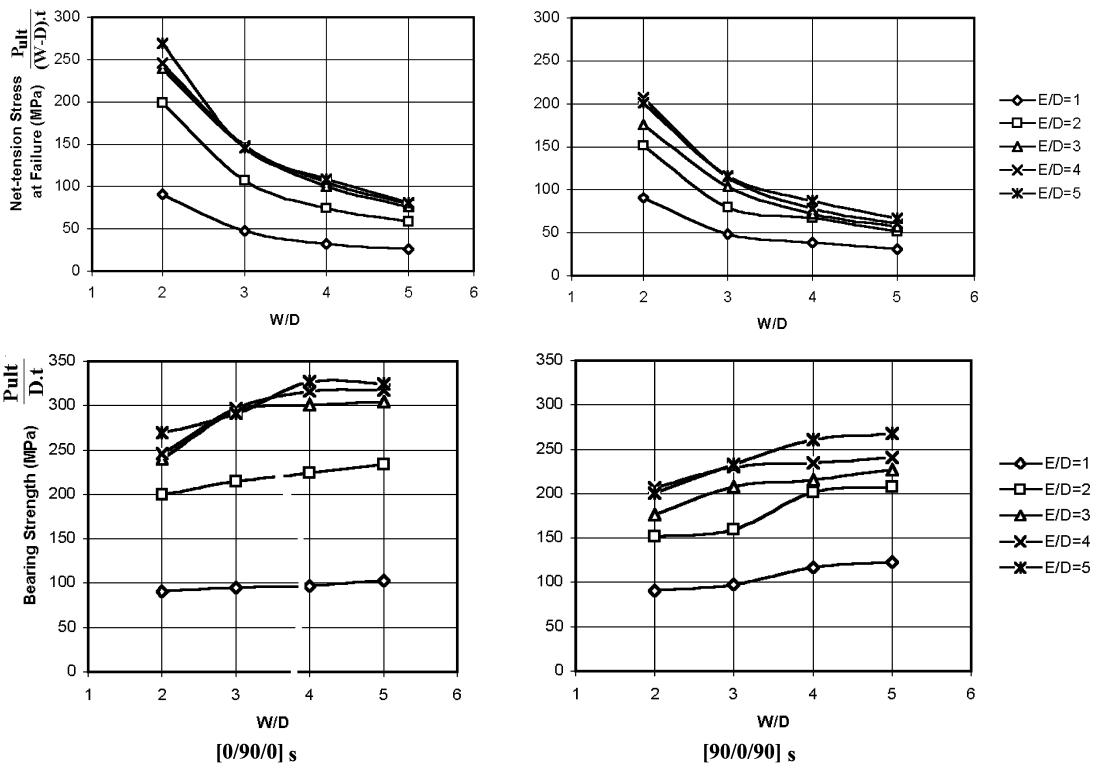

Fig. 9. The effect of width to diameter ratio on the net-tension and bearing strength for $[0/90/0]_s$ and $[90/0/90]_s$ laminates.

The effect of E/D ratio on the shearing strength and bearing strength of the $[0/90/0]_s$ and $[90/0/90]_s$ laminates are shown in Fig. 8. The bearing strength is defined as the ultimate bearing load divided by the area that is the product of pin diameter and specimen thickness. The $[0/90/0]_s$ specimens showed a sudden increase in bearing strength for E/D ratios between 1 and 3. For higher edge ratios an increase in edge distance does not seem to influence significantly the bearing strength. In contrast, the $[90/0/90]_s$ specimens showed a steady increase with E/D ratios. The effect of W/D ratio on the net-tension strength and bearing strength of the $[0/90/0]_s$ and $[90/0/90]_s$ laminates was shown in Fig. 9. It is evident from the data presented in Fig. 9 that the bearing strengths are influenced by the value of W/D for $[90/0/90]_s$ laminate with $E/D = 1$. Whereas the various W/D ratios do not have any important effect on the bearing strength for $[0/90/0]_s$ laminate with small E/D, and the bearing strength is almost independent of W/D. For high E/D ratios, the bearing strengths are nearly the same when W/D ratio is equal or greater than 4. It is clear that the $[0/90/0]_s$ laminates containing a large percentage of 0° layers are noticeably stronger than $[90/0/90]_s$ laminate. The deflection at a low load level may be due to the early failure of 90° layers in the $[90/0/90]_s$ laminate. The bearing strength shows an increase of about 24% for the $[0/90/0]_s$ lay-up compared with the $[90/0/90]_s$ lay-up for $E/D = 5$ and $W/D = 5$. It is also observed that the differences between shear strengths and net-tension strengths for the two laminates are nearly the same.

5.2. Comparison of experimental and numerical results

Bearing strengths were compared for $E/D = 1$ to 5, with $W/D = 2$ to 5 for linear, non-linear and experimental cases. $[0/90/0]_s$ laminate was chosen for comparison. By comparing the results of the failure analysis for linear and non-linear cases and the experimental results, the following points are observed.

When examining Fig. 10, three conclusions are obvious. First, it is clear that the material non-linearity has an influence on the bearing strength. Second, the non-linear model predicts very well for data in all ranges except for $E/D = 1$, and it is especially good that the results in the bearing range of failure are close to experimental values. Third, the linear model gives close results at the lower end of the W/D and E/D scales.

Since the linear model gives less accurate results, only the bearing strengths are compared for non-linear and experimental cases. As the $E/D = 1$ to 5 and $W/D = 2$ to 5, the effects of ply orientation on bearing strength were shown in Fig. 11. A comparison was performed between $[0/90/0]_s$ and $[90/0/90]_s$ laminates. The difference between the two laminates was the ratio of 0° plies. The failure mode and failure extension were apparently governed by the ply orientation in each direction. The increase of the ratio of 90° plies results in extended failure along the width of specimen

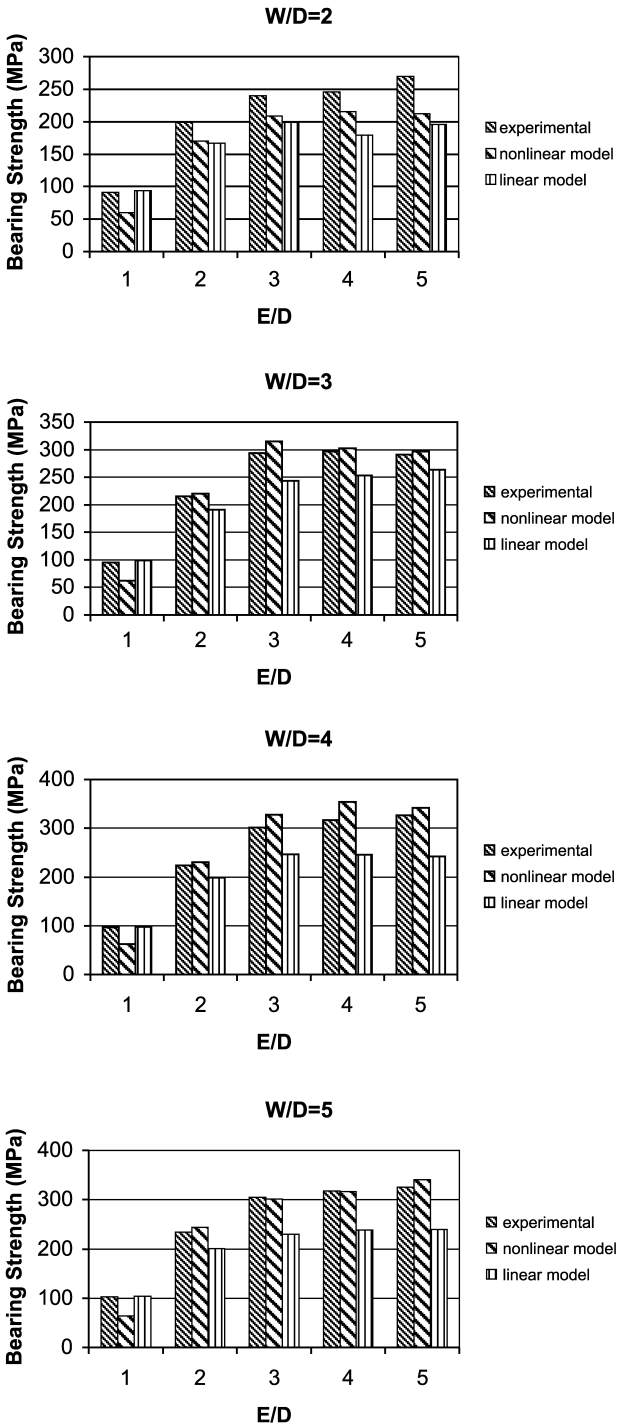

Fig. 10. Variation of bearing strength of $[0/90/0]_s$ with $W/D = 2$ to 5.

due to axial tension, whereas the decreasing of the ratio of 90° layers prevents such failure. From Fig. 11, it can be seen that the results of non-linear model agree well with the test results. But only the predicted bearing strengths for $[0/90/0]_s$ and $[90/0/90]_s$ laminates are smaller than those of achieved from tests carried out on the same laminate when W/D is increased from 2 to 5 and $E/D = 1$ held constant. It is worth noticing that the bearing strength is relatively constant over a critical width and end distance.

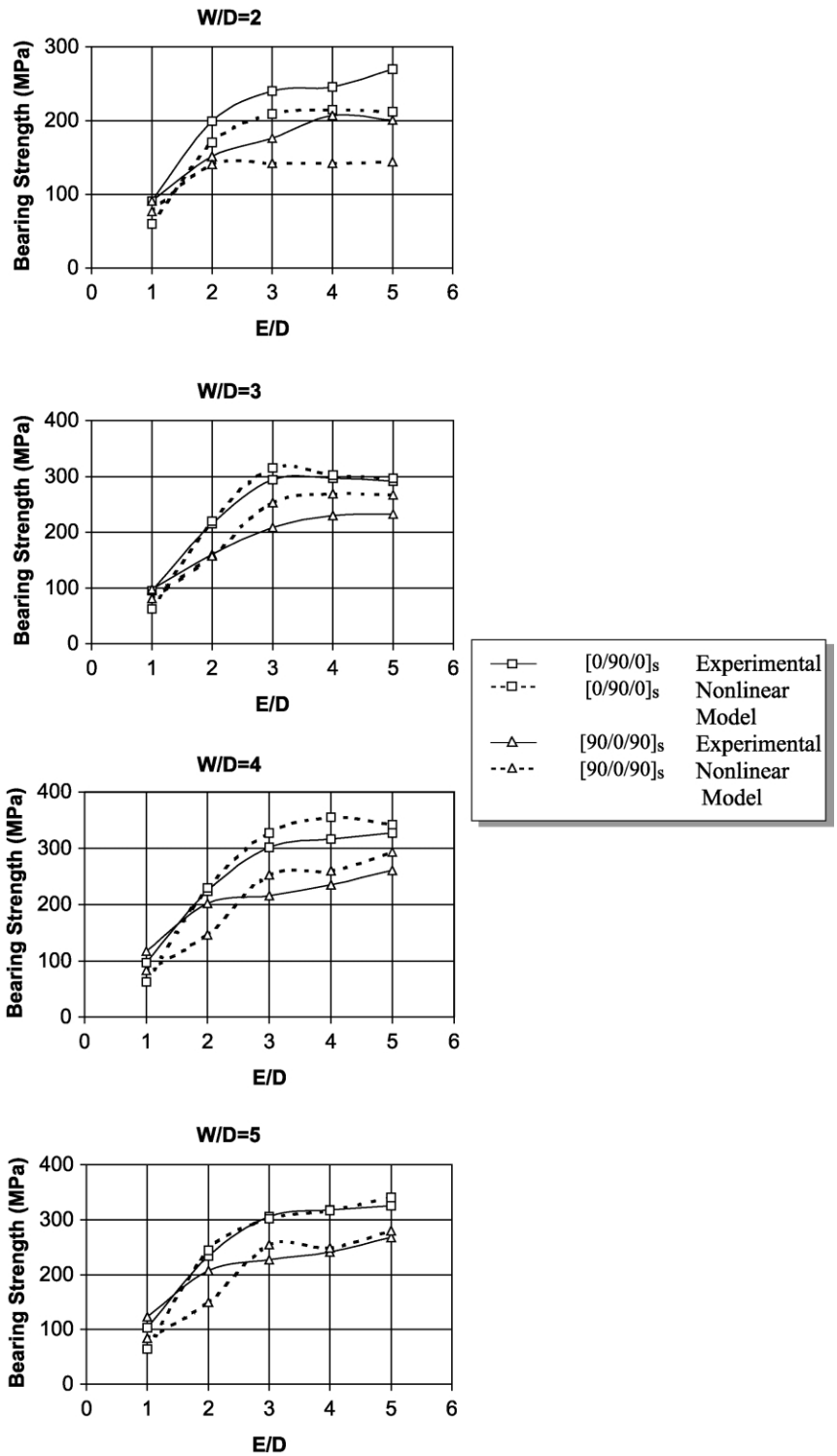

Fig. 11. Comparison of $[0/90/0]_s$ and $[90/0/90]_s$ laminates.

6. Conclusion

This work has explained the effect of geometric factors and material parameters on failure loads and mechanisms of a pin-loaded E-glass/epoxy laminates with $[0/90/0]_s$ and $[90/0/90]_s$ lay-ups. The width of the plate and distance from the upper edge of the plate to the hole center were taken as geometric factors.

- The finite element and experimental joint responses show good correlation. Configurations corresponding to specimen with small *W*/*D* and/or *E*/*D* ratios resulted in the greatest deviation from the values determined experimentally. Finite element modeling predicts final failure load usually to within 10% of experimental values for $[0/90/0]_s$ laminate while for $[90/0/90]_s$ laminate the percent difference is slightly higher.
- The in-plane shear non-linearity greatly affects laminate's mechanical response in a pin-loaded condition. The numerical solutions including non-linearity were in good agreement with the test results. The bearing strengths at the bigger *W*/*D* and *E*/*D* scales are close to experimental values.
- Joint failure with the net-tension and shear-out modes is catastrophic and immediate. But bearing failure is progressive. For this reason, bearing failure is preferred in applications. Shear-out failure is prevalent for fiber patterns that are both predominantly in 0° and deficiently in 90° plies. The dependence of the critical end distance on width deserves more investigation.
- Full bearing strength, for pinned joints, is only developed if failure due to tension and shear is suppressed by providing sufficiently large end distance and width. Very wide joints will fail in bearing. As the width is reduced, the failure mode will eventually change to tension. The width at which the mode change occurs will depend on the lay-up. Changing end distance has the same effect on the shear-out failure as width has on the net-tension failure. Clearly a joint must have adequate end distance if it is to achieve its full bearing strength.
- The failure modes change to bearing mode for both of the cases as *W*/*D* and *E*/*D* became higher. For the $[0/90/0]_s$ laminate, failure mode was found as bearing mode when the *E*/*D* ratio is greater than 3. For the small value of 3, the mode is found as shear-out that is a weak type of failure. A similar result was obtained for the critical *W*/*D* ratio. From the experimental results, for the $[90/0/90]_s$ laminate, it was found that the critical *E*/*D* ratio was 4 for $W/D = 2$ and 3 and the critical *E*/*D* ratio was about 2 for $W/D = 3$ and 4. Prior to reaching the critical *E*/*D* values, net-tension failure was observed in all specimens except for those with $E/D = 1$, which displayed a shear-out failure mode.
- It was shown that, the net-tension strength of single-hole joints is strongly dependent on the ply orientation within the laminate and specimen width.
- Looking at the shear performance of single-hole joints, it can be said that the shear strength is dependent on ply orientation and edge distance.

The results presented in this paper can be used in the design of mechanically fastened joints involving fiber reinforced laminates such as $[0/90/0]_s$ and $[90/0/90]_s$.

References

[1] De Jong T. Stresses around pin-loaded holes in elastically orthotropic or isotropic plates. J Compos Mater 1977;11:313–31.

[2] Lekhnitskii SG. Anisotropic plates. London: Gordon and Breach; 1998.

[3] Waszczak JP, Cruse TA. Failure mode and strength predictions of anisotropic bolt bearing specimens. J Compos Mater 1971;5:421–5.

[4] Matthews FL, Wong CM, Chryssafitis S. Stress distribution around a single bolt in fiber-reinforced plastic. Composites 1982; July: 316–22.

[5] Chang FK, Scott RA, Springer GS. Strength of mechanically fastened composite joints. J Compos Mater 1982;16:470–94.

[6] Chang FK. The effect of pin load distribution on the strength of pin loaded holes in laminated composites. J Compos Mater 1986;20: 401–8.

[7] Lin CC, Lin CH. Stresses around pin-loaded hole in composite laminates using direct boundary element method. Int J Solids Struct 1999;36:763–83.

[8] Lessard LB, Shokrieh MM. Two-dimensional modeling of composite pinned-joint failure. J Compos Mater 1995;29:671–97.

[9] Camanho PP, Matthews FL. A progressive damage model for mechanically fastened joints in composite laminates. J Compos Mater 1999;33:2248–80.

[10] Hassani F, Shokrieh MM, Lessard LB. A fully non-linear 3D constitutive relationship for the stress analysis of a pin-loaded composite laminate. Compos Sci Technol 2002;62:429–39.

[11] Sun HT, Chang FK, Qing X. The response of composite joints with bolt-clamping loads. Part I. Model development. J Compos Mater 2002;1:47–92.

[12] Iarve E. Three-dimensional stress analysis in laminated composites with fasteners based on the B-spline approximation. Composites, Part A 1997;28A:559–72.

[13] Camanho PP, Matthews FL. Delamination onset prediction in mechanically fastened joints in composite laminates. J Compos Mater 1999;10:906–27.

[14] Li H-C, Chang FK. Strength envelope of bolted composite joints under bypass loads. J Compos Mater 1996;30:1402–34.

[15] Collings TA. The strength of bolted joints in multi-directional CFRP laminates. Composites 1977;43–55.

[16] Hart-Smith LJ. Mechanically fastened joints for advanced composites—phenomelogical considerations and simple analysis. In: Leneo EM, Oplinger DW, Burke JJ, editors. Fibrous composites in structural design. New York: Plenum Press; 1980.

[17] Chen JC, Lu CK, Chiu CH, Chin H. On the influence of weave structure on pin-loaded strength of orthogonal 3D composites. Composites 1994;25:251–62.

[18] Abd-El-Naby SFM, Hollaway L. The experimental behaviour of bolted joints in pultruded glass/polyester material. Part 1. Single-bolt joints. J Compos Mater 1993;24:531–8.

[19] Quinn WJ, Matthews FL. The effect of stacking sequence on the pin-bearing strength in glass fiber reinforced plastic. J Compos Mater 1977;11:139–45.

[20] Maikuma H, Kubomura K. Bearing strength and damage progress for PAN-based and pitch-based carbon fiber composites. J Compos Mater 1993;27:1739–61.

[21] ASTM 3039-76, Test method for tensile properties of fiber-resin composites. American Society for Testing of Materials; 1982.

[22] ASTM 5379, Test method for shear properties of composite materials by the V-notched beam method. American Society for Testing of Materials; 1996.

[23] Tsai HH, Morton MY, Farley GL. An experimental investigation of Iosipescu specimen for composite materials. J Exp Mech 1991; 328–36.

[24] Hahn HT. Nonlinear behavior of laminated composites. J Compos Mater 1973;7:257–71.

[25] ASTM D 3518-76, In-plane shear stress–strain response of unidirectional reinforced plastics. American Society for Testing of Materials; 1982.
[26] Jones RM. Mechanics of composite materials. Tokyo: McGraw-Hill; 1998.
[27] Okutan B, Aslan Z, Karakuzu R. A study of the effects of various geometric parameters on the failure strength of pin-loaded woven-glass-fiber reinforced epoxy laminate. Compos Sci Technol 2001;61:1491–7.
[28] Okutan B. Stress and failure analysis of laminated composite pinned joints. PhD Thesis. Izmir (Turkey): Department of Mechanical engineering, Dokuz Eylul University; December 2001.
[29] Aktaş A, Karakuzu R. Failure analysis of two dimensional carbon-epoxy composite plate pinned joint. Mech Compos Mater Struct 1999; 6:347–61.
[30] Hashin Z. Failure criteria for unidirectional fiber composites. J Appl Mech 1980;47:329–34.